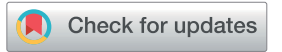
Sustainable Energy & Fuels



PAPER

View Article Online
View Journal | View Issue



Cite this: Sustainable Energy Fuels, 2022, 6, 2314

Experimental-based mechanistic study and optimization of hydrothermal liquefaction of anaerobic digestates†

Hanifrahmawan Sudibyo, (10 *abc Matteo Pecchi (10 ab and Jefferson William Tester (10 ab

Valorization of agricultural and food waste digestates is crucial for sustainable waste management to reduce environmental impacts and improve the economics of commercial farms. Hydrothermal liquefaction (HTL) of anaerobic digestates was evaluated to recover resources by converting them into carbon-dense biocrude oil and a nutrient-rich HTL aqueous phase (HTL-AP) coproduct. The effects of HTL temperature (280-360 °C), reaction time (10-50 min), feedstock pH (2.5-8.5), digestate salt content (1-5 wt%), and digestate cellulose-to-lignin ratio (0.2-1.8) on energy and nutrient recovery were systematically investigated in a set of well-designed experiments following a half-fractional central composite protocol. Response surface analysis combined with HTL product characterization and comparative literature study produced a comprehensive reaction pathway for HTL of anaerobic digestates. Moreover, this analysis revealed the importance of acidic feedstocks (pH 3.00-5.53), high reaction temperatures (337-360 °C), and reaction times <45 or 45-50 min for digestates with Cel/Lig >1 or <1, for maximizing the energy recovered in biocrude (high carbon yield and low heteroatom content) and the amounts of P, NH₃-N, and Mg distributed in the HTL-AP. Acidic conditions catalyzed biocrude production, inhibited the Maillard reaction (lowering the nitrogen content in biocrude), and partitioned nutrients into the HTL-AP. Higher reaction temperatures coupled with longer reaction times activated hydro-denitrogenation and deoxygenation reactions to improve biocrude quality. This work provides not only validated methods to achieve targeted resource recovery for specific feedstock compositions using HTL, but also a comprehensive mechanistic understanding of the HTL of biomass waste for controlling target product characteristics.

Received 15th February 2022 Accepted 30th March 2022

DOI: 10.1039/d2se00206j

rsc.li/sustainable-energy

1. Introduction

Widespread implementation of intensive industrial agricultural systems and accelerated development of refined food products to meet the increasing global demand generate substantial wet biomass waste. For example, in the livestock cattle farming industry (including beef, dairy cows, and other types of cattle), approximately, 300 million tons of dry manure is produced annually (equivalent to \sim 3 billion tons of wet manure assuming an average 90% moisture content) from 94 million cattle raised in 882 692 cattle/calf farms in the U.S.¹ According to the Environmental Protection Agency's 2018 Wasted Food Report, approximately 103 million tons of food is wasted annually by

Anaerobic digestion (AD) including anaerobic co-digestion has been widely used to convert agricultural and food wastes into methane-rich biogas.³ The biogas can be used for fuel, heat, and power generation, and can be injected into the natural gas grid after purification. Despite its advantages, AD produces a residual waste stream called anaerobic digestates – a wet mixture of organic and inorganic matrices rich in non-digested lignocellulosic fibers and nutrients whose compositions strongly depend on the characteristics of the substrates fed into the digester.⁴

Anaerobic digestates are commonly spread on agricultural fields and pastures and incorporated into the soil as an amendment/fertilizer. If mismanaged, this approach can potentially emit greenhouse gases,⁵ form air-polluting ammonium aerosol salts,⁴ cause phytotoxicity in plants,⁶ spread pathogens,⁷ and cause eutrophication and acidification in water basins due to N and P leaching and runoff from soil.⁸ This calls for a more sustainable digestate management method, possibly in alignment with a circular bio-economy approach.

Hydrothermal liquefaction (HTL) is an attractive thermochemical process for the conversion of wet biomass waste (e.g.,

the industrial, residential, institutional, and commercial sectors in the U.S.²

[&]quot;School of Chemical and Biomolecular Engineering, Cornell University, Ithaca, NY 14850. USA

^bEnergy Systems Institute, Cornell University, Ithaca, NY 14850, USA. E-mail: hs987@ cornell.edu

^cChemical Engineering Department, Universitas Gadjah Mada, Yogyakarta 55281, Indonesia

[†] Electronic supplementary information (ESI) available. See DOI: 10.1039/d2se00206j

anaerobic digestates) into biocrude oil, a solid hydrochar, and an aqueous-phase (HTL-AP) coproduct. Compared to other thermochemical routes like pyrolysis and gasification, HTL is conducted in a pressurized liquid aqueous phase at temperatures above the boiling point of water but far below typical pyrolysis temperatures. Importantly, it does not require an energy-intensive pre-drying step.9,10 HTL provides an activated environment for reformative chemistry in water near or above its critical temperature of 374 °C. Under near-supercritical conditions (280-360 °C and 10-20 MPa), the dielectric constant of water decreases from 80 at 25 °C to 15 at 360 °C, and the ionic product of water (K_w) is on the order of 10^{-12} to 10^{-11} at 280-360 °C, two to three orders of magnitude higher than that at 25 °C (10⁻¹⁴).9 The lower water dielectric constant enables easier solubilization of less-polar compounds, and its higher ionic product increases its ionic reactivity, making it both an acid and a base catalyst.

An important branch of HTL research has focused on maximizing the biocrude yield and carbon content while minimizing its heteroatom (i.e., O and N) and nutrient (e.g., NH₃-N, P, K, Ca, and Mg) contents to facilitate coprocessing of HTL biocrude with conventional crude in petroleum refineries. The HTL temperatures between 310 and 350 $^{\circ}\text{C}$ and the reaction times between 15 and 60 min have been reported to maximize the biocrude yield and minimize the biocrude heteroatom content from a variety of feedstocks, 11-14 while homogeneous and heterogeneous catalysts have been reported to increase the carbon content in biocrude by catalyzing deoxygenation and denitrogenation reactions.15-18

Another branch of HTL research has instead focused on recovering nutrients from HTL products in the form of inorganic fertilizers, for example, struvite (MgNH₄PO₄·6H₂O) crystallization from the HTL-AP under alkaline conditions to produce a slow-release inorganic fertilizer providing plantavailable P, N, and Mg. 19,26,27 To maximize struvite production from the HTL-AP, nutrients in the feedstock should preferentially partition in the HTL-AP, where they tend to assume their bioavailable forms (e.g., NH₄⁺, orthophosphates, K⁺, Ca²⁺, and Mg²⁺) rather than accumulate in the hydrochar phase in their non-bioavailable forms (e.g., apatite phosphate, 19 calcite, 20 and vivianite21). Since struvite formation is inhibited by the presence of Ca ions, the Ca concentration in the HTL-AP should be minimized, as it would cause the formation of a morethermodynamically stable hydroxyapatite (a less effective Pfertilizer).22 Increasing the HTL reaction temperature and/or reaction time has been reported to enhance the distribution of calcium and multivalent metals into the hydrochar and increase the NH3-N yield in the HTL-AP.23 Moreover, preacidification of the feedstock to pH 2-4 maximizes N and P partitioning into the HTL-AP.19,24

The feasibility and sustainability of HTL for sustainable resource recovery depend on the economic values and environmental benefits of the products generated. In this context, process conditions should be specified to simultaneously achieve the following targets: (1) maximum biocrude energy recovery, (2) low biocrude heteroatom content, (3) maximum yield of Mg, NH₃-N, and P in the HTL-AP, and (4) minimum

yield of Ca in the HTL-AP. Specifying desirable HTL operating conditions requires a detailed understanding of the HTL reaction mechanisms, particularly those associated with the interaction between feedstock compositions and HTL operating conditions and their combined effects on HTL products.

The aim of this study is therefore twofold. The first is to provide a comprehensive mechanistic understanding of the combined effects of feedstock characteristics and process parameters on the final HTL products for digestates. The second is to establish a method for determining the HTL operating conditions that maximize energy and nutrient recovery based on various feedstock compositions. These two key goals are achieved through the following five steps:

- (1) Preparation of a set of synthetic anaerobic digestate mixtures with different compositions (pH, salt content, and cellulose-to-lignin ratio).
- (2) Design of an HTL experiment matrix using a response surface methodology (RSM) based on a half-fractional central composite design (HFCCD) to describe the effects of digestate compositions and HTL process conditions (reaction temperature and time) on biocrude energy recovery; biocrude heteroatom (N and O) content; and mineral nutrient yield particularly Mg, NH₃-N, P, and Ca in the HTL-AP. A total of 32 HTL experiments were performed. The HTL product separation and characterization methods included filtration, extraction, elemental analysis, GC-MS, XRD, and colorimetry. Quadratic regression models for the corresponding response variables are obtained by fitting the results of the experimental analysis.
- (3) Proposal of a comprehensive HTL mechanism for digestates based on the results of the statistical analysis of the experimental outcomes and the comparative literature study.
- (4) Application of a desirability function approach²⁵ to determine a range of HTL process conditions to achieve the optimization targets. The exponential desirability function approach translates the regression equations obtained from the response surface experiment to a value between 0 (undesirable) and 1 (desirable).25 This value is obtained as the weighted (geometric) average of the contributions of each optimization target, and it gives an idea of how close a set of specific operating conditions leads to the desired overall outcomes.
- (5) Validation of the suggested HTL process conditions by the desirability function approach through additional replicated HTL experiments on different digestate compositions.

While this work deals with the optimization of the HTL-AP composition for maximum struvite production, it does not describe the struvite production as well as its optimization. A detailed investigation of struvite crystallization from the HTL-AP will be given in the forthcoming paper.

2. Materials and methods

2.1 Synthetic anaerobic digestate preparation

Typical physicochemical properties of anaerobic digestates are presented, indicating a high variability of cellulose-to-lignin (Cel/Lig) ratio, mineral salt content, and pH. The model compounds used to prepare the synthetic anaerobic digestate mixtures, including the supplier, purity, and the reasons for

Table 1 Typical anaerobic digestate compositions and rationales for pre-selected model compounds to prepare synthetic anaerobic digestate mixtures

Typical digestate compositions from the literature		Model compounds for synthetic digestate preparation					
Parameters	Ranges	Model compounds	Rationales				
Dry matter (DM), wt%	1.5–23.2 (ref. 4 and 26)	Ultrapure water (Milli-Q water)	Used to adjust the dry matter content.				
Organic, %DM	60-80 (ref. 26)	Alkaline lignin (≥94% purity, SCBT)	50-80% of organics in the anaerobic				
Cel/Lig, g g ⁻¹	0.22–1.71 (ref. 4 and 27)	Microcrystalline cellulose (≥99.99% purity, MilliporeSigma)	digestate are non-digested lignocellulosic fibers. ⁴				
Total-C, %DM	26-45 (ref. 4, 26 and 28)						
Total-N, %DM	2.4-7.6 (ref. 4 and 28)	Glutamic acid (≥99.99% purity, BioBasic)	Org-N is from amino acids (protein hydrolysis). NH ₄ is very likely to chelate				
Org-N, %total-N NH ₃ -N, %total-N	17.5–24.6 (ref. 4 and 28) 55.4–82.5 (ref. 4 and 28)	NH ₄ -acetate (≥99.99% purity, J.T. Baker)	acetate produced from the acidogenesis step. 26				
Ash, %DM	15–36 (ref. 26)	CaHPO ₄ ·2H ₂ O (≥99% purity, Eisen- Golden)	P existed mostly as CaHPO ₄ ·2H ₂ O in the digestate. ²⁹ Ca and Mg existed as CaCO ₃				
P, %DM	0.6-1.7 (ref. 26)	CaCO ₃ (≥99% purity, Loudwolf)	and MgCO ₃ , respectively, from the				
Ca, %DM	1-2.3 (ref. 4 and 26)	MgCO ₃ (≥98% purity, Aldon Corp.)	reaction with CO ₃ ²⁻ . ^{26,30} K exists as				
Mg, %DM	3–7 (ref. 4 and 26)	KCl (≥99.99% purity, EMD chemicals)	soluble halide salts in the digestate. ²⁶				
K, %DM	1.2–11.5 (ref. 4 and 26)						
рН	7–9 (ref. 4 and 26)	Acetic acid (≥99.5% purity, J.T. Baker) NaOH (100% purity, Belle chemical)	Acetic acid is used for acidification as it is the primary product from acidogenesis. ²⁶ NaOH is used to control pH in digesters. ³⁰				

their selections, are shown in Table 1. Pre-selected model compounds were mixed with ultrapure water (18.2 M Ω cm), and their compositions in the mixture for each experiment can be found in the ESI† (see Table S1). In general, the total concentration of cellulose and lignin was fixed at 8 wt%, the total concentration of amino acid and ammonium salt was fixed at 3 wt% (with NH₃–N to N_{organic} molar ratio of 3:1), and the salt content varied from 1 to 5 wt%. This resulted in a total solid loading of 12–16 wt% in the mixture. The estimated ash content on dry matter basis was 8–31% (see Table S1, ESI†), which falls within the reported values for ash content of anaerobic digestates. ²⁶

2.2 HTL procedure and product analysis

The HTL experiments used the same experimental setup and procedures as described in a previous study by our group in Fig. S1 (ESI†).20 With this setup, the heating time required to reach the target reaction temperature of 280, 300, 320, 340, and 360 °C was around 45, 50, 60, 70, and 80 min, respectively (see Fig. S19, ESI†). Meanwhile, the cooling time required to reach \sim 80 °C (where no hydrothermal reaction takes place) was consistently around 15 min (see Fig. S19, ESI†). The statistical analysis shown in Tables S15 and S16 (see ESI†) indicates that the effects of the experimental variation of the heating and cooling time due to the system setup were statistically insignificant on the HTL outcomes, compared to the effect of the other studied process parameters. Therefore, this experimental design provides an appropriate structure for the central composite design to efficiently evaluate the effects of important variables within their realistic operating ranges.

Three products were collected from each experiment: biocrude oil, hydro-char, and HTL-AP. Three biocrude extraction fractions were collected: dichloromethane-extracted and ethylacetate extracted water-soluble biocrudes (DWO and EWO), and dichloromethane-extracted solid-bound biocrude (DSO). The yield of biocrudes or hydrochar was calculated using eqn (1). The ash content in biocrudes was determined with the ASTM E1131-20 method³¹ to obtain the dry-ash-free yield of biocrude (see eqn (2)). The total biocrude oil yield was calculated as the sum of the yield of DWO, EWO, and DSO extraction fractions. The elemental content (%C_i, %H_i, %N_i, and %O_i) of biocrudes and hydrochar was measured with a CE-440 Elemental Analyzer (Exeter Analytical). The biocrude higher heating value (HHV) was calculated according to the elemental composition using the equation by Channiwala and Parikh,³² and the total energy recovery was calculated with eqn (3).

$$Y_{\rm i} = \frac{m_{\rm i}}{m_{\rm feedstock}} \times 100\% \tag{1}$$

$$Y_{\text{oil,daf}} = \frac{m_{\text{oil}} \times (1 - \% \text{Ash}_{\text{oil}})}{m_{\text{feedstock}}} \times 100\%$$
 (2)

$$ER_{oil} = \frac{m_{oil} \times HHV_{oil}}{m_{feedstock} \times HHV_{feedstock}} \times 100\%$$
 (3)

Y is the product mass yield, m is the product mass (g), i indicates biocrude oil or hydrochar, $m_{\text{feedstock}}$ is the dry mass of feedstock (g), $Y_{\text{oil,daf}}$ is the dry-ash-free mass yield of biocrude, m_{oil} is the biocrude mass (g), %Ash_{oil} is the ash content of biocrude (wt%), and ER_{oil} is the biocrude energy recovery.

The yield of carbon and nitrogen in biocrude or hydrochar was calculated using eqn (4), while their yield in the HTL-AP was calculated using eqn (5) and (6).

$$X_{\text{yield-i}} = \frac{(\%X_{\text{i}}) \times m_{\text{i}}}{X_{\text{feedstock}}} \times 100\%$$
 (4)

$$C_{\text{yield-AP}} = \frac{[\text{TOC}]_{\text{AP}} \times (V_{\text{AP}})}{X_{\text{feedstock}}} \times 100\%$$
 (5)

$$N_{\text{yield-AP}} = \frac{[\text{TN}]_{\text{AP}} \times (V_{\text{AP}})}{X_{\text{feedstock}}} \times 100\%$$
 (6)

 X_{vield} represents the mass yield of carbon or nitrogen, $\%X_i$ is the elemental content of carbon or nitrogen in biocrude or hydro-char, i indicates biocrude or hydrochar, and $X_{\text{feedstock}}$ is the mass of carbon or nitrogen in the feedstock (g). The total yield of carbon and nitrogen in biocrude (Cvield-oil or Nvield-oil) is the sum of carbon or nitrogen yield in the three biocrude extraction fractions. Meanwhile, Cvield-AP and Nvield-AP are the yield of carbon and nitrogen, respectively, in the HTL-AP, [TOC]_{AP} and [TN]_{AP} are the total organic carbon and the total nitrogen concentration (mg L⁻¹), respectively, measured using a Shimadzu TOC-L CSN, and V_{AP} is the HTL-AP volume (L).

The nutrient concentration in the HTL-AP ($[X]_{AP}$, mg L⁻¹) was measured colorimetrically (Hanna Instruments HI83399). NH₃-N, P, K, Cl, Mg, and Ca were determined with the ASTM D1426-15,33 amino acid,34 tetraphenylborate,35 mercury(II) thiocyanate,36 calmagite,37 and oxalate38 methods, respectively. The nutrient yield in the HTL-AP (Z_{AP}) was calculated with eqn (7) based on colorimetrically measured nutrient concentration $([Z]_{AP}, \text{ mg L}^{-1} - \text{using a HI83399 photometer from Hanna})$ Instruments) where Z represented any one of NH₃-N, P, Mg, and Ca, V_{AP} is the HTL-AP volume, and $Z_{feedstock}$ is the mass of Z in the feedstock (g).

$$Z_{\rm AP} = \frac{[Z]_{\rm AP} \times V_{\rm AP}}{Z_{\rm feedstock}} \times 100\% \tag{7}$$

The yield of nutrient (Z – Mg, P, or Ca) in the hydrochar (Z_{HC}) was calculated using eqn (8) where $\%Z_{HC}$ is the nutrient content of the hydro-char measured using energy dispersive X-ray spectroscopy (Oxford Instruments)

$$Z_{\rm HC} = \frac{\% Z_{\rm HC} \times m_{\rm HC}}{Z_{\rm feedstock}} \times 100\% \tag{8}$$

GC-MS compositional analysis (Agilent 6890N GC with a JEOL JMS-GCMATE II MS) was performed on selected biocrude samples (GC-MS operating conditions and procedure are given in Table S6, ESI†) to semi-quantify the presence of organic compounds. The thermogravimetric analysis (TGA) was also performed by heating 10-20 mg of selected biocrude samples from room temperature to 700 °C at 10 °C min⁻¹ in 50 mL min⁻¹ of atmospheric nitrogen (TA Instruments QA500). The TGA results given in Fig. S20 and S21 (ESI†) showed that 60-80% components in the biocrude samples have a boiling point ≤300 °C; thus, the majority of chemical compounds in the biocrude were detectable using the adopted GC-MS procedure.

The HTL-AP was also analyzed for the organic compositions with GC-MS, which was performed similarly to that for biocrude with pre-derivatization following the methyl-chloroformate method.³⁹ In addition, the liquid-phase product was measured for pH to determine pH change after reaction (Δ pH_{liq}). To investigate the phase transformation of precipitated mineral nutrients, the hydrochar mineral compositions were characterized with XRD (Bruker D8 Advance ECO).

2.3 Structure of the experiments and modelling

2.3.1 Design of experiments. A composite design following the HFCCD protocol⁴⁰ was adopted to explore all combinations of independent variables systematically and practically, i.e., reaction temperature and time, feedstock pH, salt content, and cellulose-to-lignin ratio. The HFCCD is constructed on a twolevel (factor level -1 and 1) half-factorial design added with a center point (factor level 0) and a group of axial points (factor level -2 and 2), making each factor has five levels. To investigate the five independent variables in this study, the HFCCD generated thirty-two sets of HTL experiments (see the full design matrix in Table S2, ESI†) comprising sixteen halffactorial points, ten axial points, and one five-time-replicated center point to assess reproducibility.

The selected ranges for the investigated operating conditions (see Table 2) were selected to gain a mechanistic understanding of the elemental distribution in the major products. Reaction temperatures of 280–360 °C were chosen because this range has been reported to produce the highest biocrude and nutrient vields. 41 Reaction times of 10-50 min were selected as this range has been reported to provide a total conversion of biomass.41 The selected ranges for feedstock compositional parameters cover the typical physicochemical properties of anaerobic digestates (see Table 1). The range for feedstock pH was determined according to the typical pH of anaerobic digestate (pH 7-9, see Table 1) and the preferred pH for acidic depolymerization of lignin (pH 2-6).42 The ranges for salt content and Cel/Lig ratio were based on the reported values for various anaerobic digestates (see Table 1). Data on measured responses (see the response variables in subsection 2.2) were fitted with a quadratic regression equation (see eqn (9))40 with independent variables standardized on the factor level scale (coded units).

$$F = \alpha_0 + \sum_{i=1}^n \alpha_i X_i + \sum_{i=1}^n \alpha_{ii} X_i^2 + \sum_{i=1}^{n-1} \sum_{j=i+1}^n \alpha_{ij} X_i X_j$$
 (9)

F is the response variable, α_0 is the constant, X is the independent variable, and α_i , α_{ii} , and α_{ij} are the coefficient of linear, quadratic, and interaction terms, respectively. The equations in coded units were statistically analyzed in Minitab 19.2.0. Only statistically significant factors/terms (p < 0.05) were included in the equation. The model's adequacy was determined with R^2 , R^2 (pred.), and lack-of-fit p-value.

Multi-response optimization based on the generated regression equations was performed in Minitab 19.2.0 using the desirability function approach. 25 For different salt contents and Cel/Lig ratios in the digestate, the desirability function approach computed the optimal values of the independent

Table 2 Simple design matrix for HTL experiments⁴⁰

	Factor levels								
Independent variables	-2	-1	0	1	2				
X_1 . Reaction temperature (°C)	280	300	320	340	360				
X_2 . Reaction time (minute)	10	20	30	40	50				
X ₃ . Feedstock pH	2.5	4	5.5	7	8.5				
X ₄ . Salt content (wt%)	1	2	3	4	5				
X_5 . Cel/Lig ratio	0.2	0.6	1	1.4	1.8				

variables (reaction temperature, reaction time, and feedstock pH) that can achieve the optimization targets: (1) maximum biocrude energy recovery, (2) low biocrude heteroatom content, (3) maximum yield of Mg, NH₃-N, and P in the HTL-AP, and (4) minimum yield of Ca in the HTL-AP. All targets were given an equal weighting factor because we assumed that both biocrude and the nutrient-rich HTL-AP have the same potential economic values and environmental benefits. To validate the accuracy of this procedure, synthetic anaerobic digestates with four different compositions covering the whole spectrum of the optimization were processed using the computed optimum HTL process conditions in five-time-replicated HTL experiments. Both experimental and predicted (using the regression equations) results of the response variables obtained for each digestate composition were compared.

2.3.2 Treatment of experimental results and mechanistic modelling. The presentation of the results of our study is divided into two parts: (i) an experiment-based HTL mechanism and (ii) optimization and validation of HTL operating conditions. The first part describes the combined effects of digestate characteristics and HTL parameters on the final products and proposes comprehensive HTL reaction mechanisms for the digestate. This part relies on the results of the statistical analysis of the response variables and on their comparison with the available literature to draw mechanistic understanding. The second part deals with the optimization of HTL conditions based on digestate composition with the aim of maximizing energy and nutrient recovery. The validation of the proposed approach through additional HTL tests is also presented in the second part.

Experimental-based HTL mechanism

This section discusses the effects of the independent variables on the d.a.f. oil yield, heteroatom content in DSO (dichloromethane-extracted solid-bound biocrude) and DWO (dichloromethane-extracted water-soluble biocrude) biocrude products, and nutrient yield in the HTL-AP. This is done through a regression analysis of the experimental results from the thirty-two runs in the HTL experiment matrix, providing regression equations for all the independent variables.

In order to allow the reader to compare the relative influence of each independent variable on the response variables, Table 3 collects the coefficients for each significant term in the

equations for all response variables (eqn (9)) including the statistics, i.e., R^2 , R^2 (pred.), and the lack-of-fit p-value. The coefficients refer to the coded units (standardized variables), thus allowing a direct comparison of the coefficients. The pvalues for each significant term are reported in Tables S3-S5 (ESI†). Furthermore, to show the response variable's critical points (e.g., maxima, minima, or saddle point) as functions of the independent variables, representative contour plots are presented in the following subsection. These plots are obtained by varying two statistically significant variables in the regression equations and keeping the other variables constant at factor level zero (see the natural value of factor level zero in Table 2). A complete list of the plots is reported in Fig. S2-S12 (ESI†).

Based on the statistical analysis of the experimental results and the comparison with the literature, we proposed comprehensive HTL reaction pathways for anaerobic digestates that are summarized in Fig. 1. Each reaction pathway in Fig. 1 is labelled using the convention r#, where # is the reaction code. When a reaction pathway is discussed in the following subsections, the code is placed next to the corresponding text to allow an easier referencing to Fig. 1.

The proposed reaction pathway for the conversion of organics focused on the chemical compound formation in the biocrude and aqueous-phase products, which accounted for 55.9-95.2% of the overall mass balance, 60.2-96.0% of the carbon balance, and 54.4-92.1% of the nitrogen balance. Similarly, the proposed distribution pathway for the inorganics focused on their partitioning between hydrochar and the aqueous-phase coproduct since 95.52-99.75% of P, 97.19-99.75% of Ca, and 94.81-99.87% of Mg in the digestate were distributed into these two product phases. Comprehensive mass and elemental balances are shown in Tables S10, S11, S12, S14 and S17 in the ESI.†

3.1 D.a.f. oil yield

The measured total oil yield was 7.03-55.80% with an ash content of 1.51-9.71%; the d.a.f. oil yield was 5.52-51.80%. Among the three biocrude extraction fractions, DSO contributed 60-80% of the d.a.f. oil yield (Yoil.daf), followed by DWO 20-35% and EWO <5%. The carbon yield in biocrude (Cyield-oil) varied between 9.23 and 54.8%, 1.21 and 19.24%, and 0.27 and 13.82% for DSO, DWO, and EWO biocrude fractions, respectively, resulting in total energy recovery (ERoil) of 10.1-76.1%. The HHV of biocrudes ranged between 15 and 32 MJ kg⁻¹, similarly to previously reported values. 43,44 From the coefficient of each term in the regression model of Yoil,daf, Cyield-oil, and ERoil (see Table 3), all factors except reaction time had similar effects on these three response variables, thus indicating that the amounts of carbon and energy recovered were strongly associated with the amount of biocrude oil produced. For a comprehensive understanding of the effects of the statistically significant factors (p < 0.05) on biocrude production, reaction mechanisms based on chemical compositions in the biocrude are discussed, with a focus on the DSO and DWO fractions because of their major contributions to $Y_{\text{oil.daf}}$.

Table 3 Regression coefficients (truncated to three decimal places) for all measured response variables (see Tables S3-S5 in the ESI for untruncated coefficient values and a complete statistical assessment of the regression models)

	Measured response variables											
Terms	$Y_{\text{oil,daf}}$ (%)	C _{yield-oil} (%)	ER _{oil} (%)	$\Delta p H_{liq}$	%O _{oil-DWO}	%O _{oil-DSO}	%N _{oil-DWO}	$%N_{oil\text{-DSO}}$	NH ₃ -N _{AP} (%)	P _{AP} (%)	Mg _{AP} (%)	Ca _{AP} (%)
Constant	40.063	69.46	66.463	-0.566	60.341	22.892	0.879	2.115	34.298	17.027	64.540	32.416
T	2.390	5.789	6.577	-0.033	-2.705	-1.324	-0.026	0.058	-0.878	0.766	1.540	-1.917
T	_	_	1.658	-0.021	-1.299	-1.125	0.004	0.029	-0.584	-0.33	-0.750	-0.670
pН	-6.664	-8.94	-9.529	-0.491	-0.522	-1.600	0.087	0.373	-4.332	-12.673	-11.804	-8.552
Salt	-4.883	-4.272	-4.034	0.194	-0.947	-0.844	0.145	0.025	_	-5.807	-6.620	-2.523
Cel/Lig	1.508	3.96	3.377	-0.204	-0.187	-1.590	0.014	0.237	-2.924	5.708	_	2.331
T^2	-1.188	-2.305	-2.090	-0.099	_	_	-0.06	-0.257	2.687	_	-5.364	_
t^2	_	_	_	_	_	_	-0.057	0.244	2.110	_	-2.540	_
pH^2	-6.254	-11.636	10.852	0.143	1.215	0.867	_	_	1.041	7.624	_	-1.773
Salt ²	_	_	_	_	_	_	0.018	0.207	_	_	_	_
Cel/Lig ²	_	_	_	_	_	_	_	_	-2.219	_	_	_
$T \times t$	_	_	_	_	-0.112	-0.813	_	_	-1.453	2.677	_	2.218
$T \times pH$	_	_	_	_	_	_	_	_	1.910	_	_	_
$T \times Salt$	_	_	_	_	-0.224	-0.838	_	_	_	_	_	_
$t \times pH$	_	_	_	_	0.016	0.798	_	_	_	_	_	_
$t \times \text{Cel/Lig}$	_	_	_	_	0.448	0.959	_	_	_	_	_	_
$pH \times salt$	_	_	_	_	_	_	0.002	0.036	_	4.984	7.794	-1.988
$pH \times Cel/Lig$	1.461	2.360	_	-0.213	0.284	1.083	_	_	_	-4.805	_	_
$Salt \times Cel/Lig$	_	_	_	_	0.250	0.779	_	_	_	-4.609	_	-2.222
R^2	97.59%	94.68%	96.07%	89.41%	83.44%	85.63%	90.01%	99.14%	89.51%	97.49%	89.77%	93.53%
R^2 (pred.)	93.57%	88.31%	91.00%	73.92%	75.29%	76.55%	65.98%	97.48%	67.58%	93.21%	79.29%	80.21%
Lack-of-fit's <i>p</i> -value	0.173	0.190	0.300	0.206	0.335	0.363	0.340	0.452	0.505	0.254	0.385	0.085

3.1.1 Effect of feedstock pH. Feedstock pH was the most significant factor for biocrude formation as indicated by the largest coded coefficient of its linear and quadratic terms (see Table 3). In general, a more acidic feedstock produced a higher Y_{oil,daf}, and the yield was highest at pH around 5 (Fig. 2B). Under acidic conditions, carbohydrate monomers produced from cellulose hydrolysis were substantially converted via dehydration into furfural (r2) or 5-HMF (r1). The furfural pathway comprised isomerization (r6) and ring-opening (r8) or hydrogenation (r5) and Piancatelli rearrangement (r7) of furfural 45,46 to produce pyrones, cyclic ketones, and furanones, which were dissolved in the biocrude product-phase (see Table S7, ESI†). The 5-HMF pathway can produce the same products as the furfural pathway via decarbonylation of 5-HMF⁴⁷ (r4) followed by Piancatelli rearrangement (r7). However, the presence of levulinic acid and formic acid in the HTL-AP produced from acidic feedstocks (see Table S8, ESI†) showed that rehydration of 5-HMF (r3) also occurred. Because both decarbonylation (r4) and rehydration (r3) of 5-HMF are acid-catalyzed and can occur concurrently, 48 the maximum $Y_{\rm oil,daf}$ at a feedstock pH of \sim 5 indicated the optimum feedstock pH at which the selectivity for 5-HMF rehydration was lowest. This result is in accordance with previous studies reporting that 5-HMF rehydration in subcritical water is expedited at pH < 5,49 and was further validated by chromatography analysis of the HTL-AP produced from feedstocks with pH 2.5 and 5.5 (see Table S8, ESI†). A larger peak area percentage of levulinic acid and formic acid was observed at a feedstock pH of 2.5.

Although 5-HMF rehydration is inevitable and undesirable from an energetic perspective, the formic acid produced in this reaction might be beneficial in preventing repolymerization of lignin monomers. During acidic treatment, lignin undergoes depolymerization (e.g., acidolysis) into oil and water-soluble monomers and repolymerization into a char-like precipitate.50 Reductive depolymerization of lignin (r29) with formic acid as a hydrogen donor may block the repolymerization and increase the $Y_{\text{oil.daf}}$ from lignin via hydrogenolysis of interunit β -O-4 and α-O-4 ether bonds and removal of benzylic OH-groups to produce alkyl-substituted methoxyphenols.42,51 In addition, phenolic monomers produced from lignin acidolysis (r21) may also benefit from the presence of hydrogen donors, which allows their conversion into cyclic C6-ketones (r27).52 Both alkylsubstituted methoxyphenols and cyclic C6-ketones were nonpolar and dissolved in the biocrude product-phase (see Table S7, ESI†), and their production has been found to increase $Y_{\text{oil,daf.}}^{42}$

Phenolic compounds with a hydroxymethyl, a dioxane/ dioxolane, and a pyran structure were observed in the biocrudes produced from acidic feedstocks, e.g., 4-hydroxybenzenemethanol, 1,3-benzodioxane-5-ol, 5-(1-propenyl)-1,3benzodioxole, and 3,5,7-trihydroxy-benzopyranone (see Table S7, ESI†). The presence of a hydroxymethyl group suggests that a sufficient amount of formaldehyde readily attacked and deactivated the reactive sites of the aromatic rings during the reaction (r24).53,54 The formaldehyde may originate from lignin side chain cleavage processes during lignin acidolysis and the

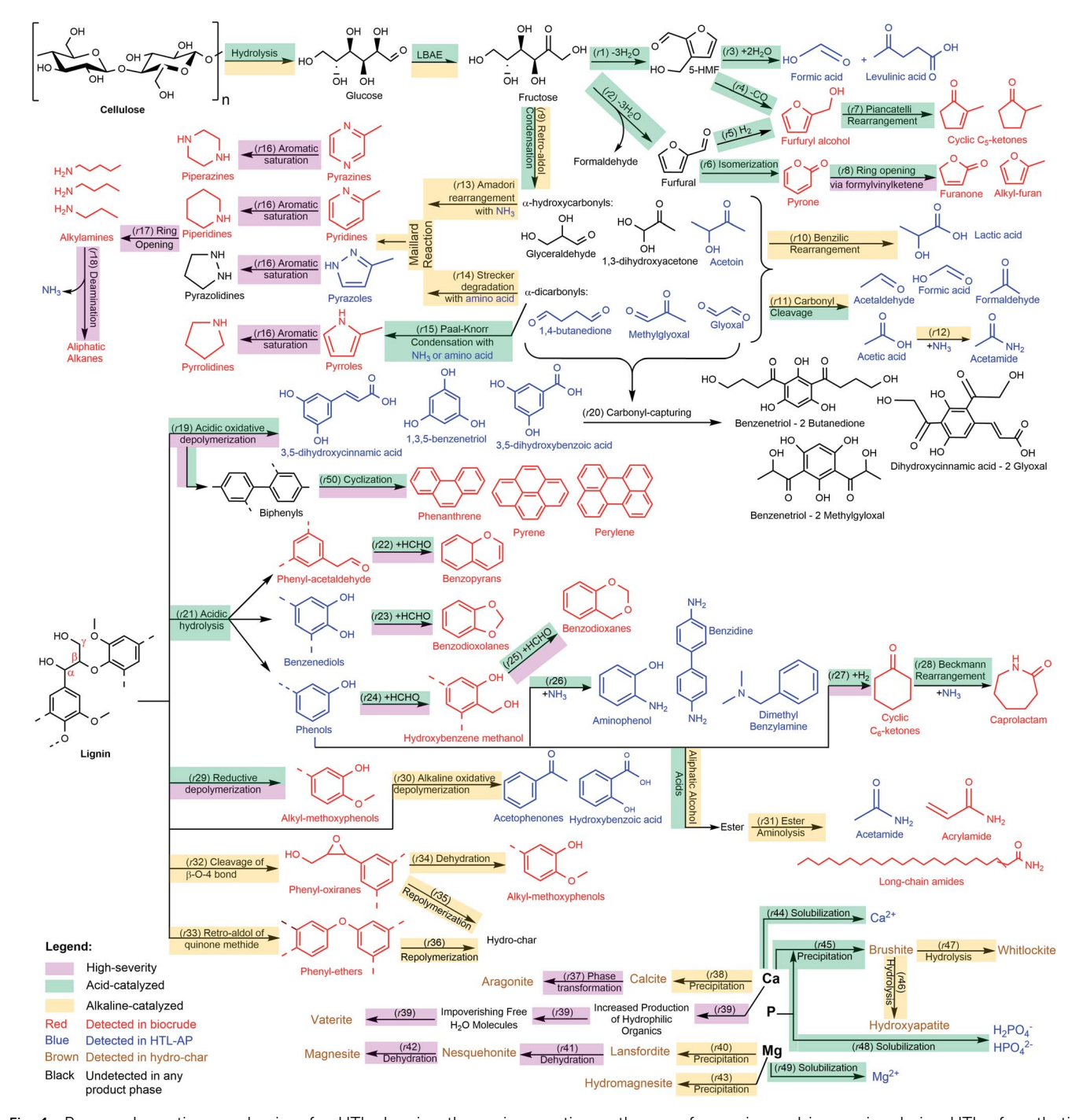


Fig. 1 Proposed reaction mechanism for HTL showing the major reaction pathways of organics and inorganics during HTL of synthetic anaerobic digestates. Each reaction pathway is labelled using r#, where # is the reaction code. The chemical structures were created using ChemDraw 20.1.1.

fragmentation of monosaccharides via acid-catalyzed retroaldol reactions.53,55 The presence of dioxane/dioxolane and pyran structures indicated stabilization of lignin monomers (i.e., C₂-aldehyde-substituted phenols and Hibbert's ketones) by the formation of cyclic acetal (r23 and r25) and pyran (r22) from the reaction between formaldehyde and the hydroxyl/ketone group of alkyl side chains on the phenyl ring. 42,54 Stabilization through hydroxymethylation and the formation of cyclic acetal and pyran restrained the repolymerization of lignin-derived biocrude into solid hydro-char, thus producing higher $Y_{\text{oil,daf}}$.

3.1.2 Effect of reaction temperature. A quadratic dependence of $Y_{\text{oil,daf}}$ was also observed on the reaction temperature although it was statistically less significant than feedstock pH (smaller coefficient value in Table 3). Raising the reaction temperature from 280 °C to 330 °C increased the Yoil,daf (Fig. 2A); thus, high reaction temperatures were required to

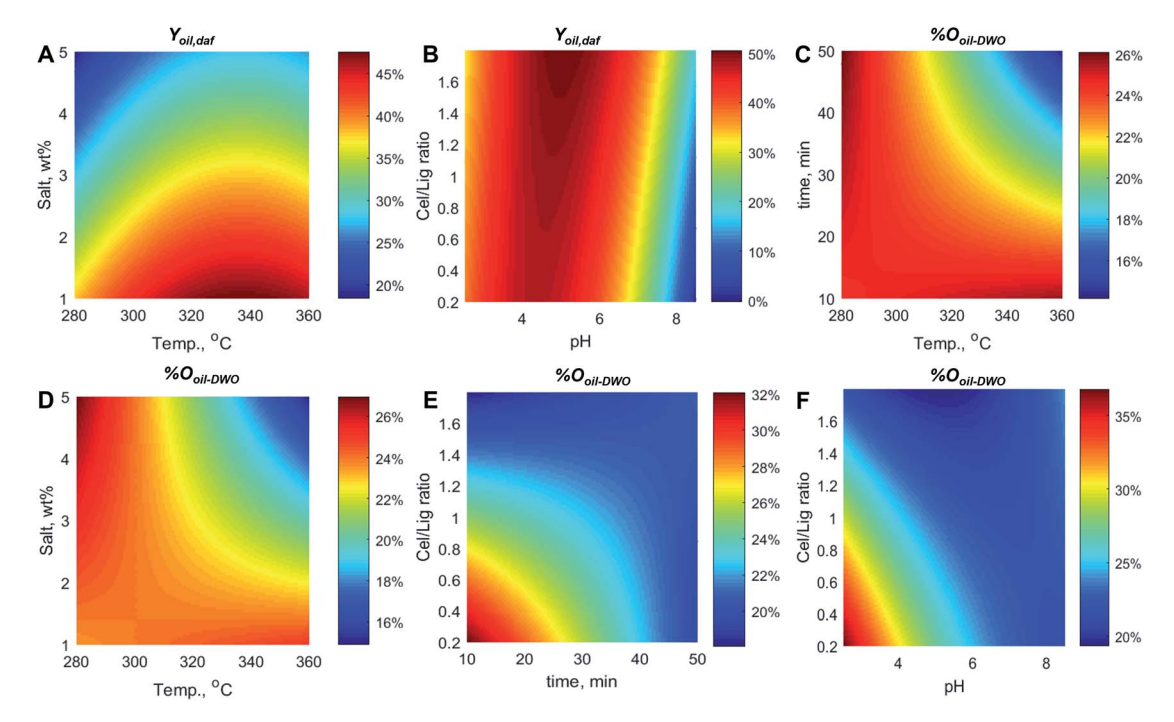


Fig. 2 Representative contour plots of d.a.f. oil yield (Yoil,daf, (A and B)) and biocrude (DSO) oxygen content (%Ooil, (C-F)).

thermochemically breakdown the recalcitrant cellulose and lignin. Moreover, high reaction temperature promoted oxidative degradation (r19) of lignin into biphenyls, which can experience cyclization and dehydration (r50) to form polyaromatic compounds,56 such as phenanthrene, pyrene, and perylene, in the biocrude phase. These non-polar polyaromatic compounds are reported to be the precursor of high boiling point compounds that are similar to those found in conventional crude oil.57 Indeed, TGA analysis of selected biocrude samples (see Fig. S20 and S21 in the ESI†) shows that 20-40% of the oil has a boiling point ≥300 °C. Nevertheless, a further increase in HTL temperature (>330 °C) gradually decreased the $Y_{\text{oil,daf}}$, owing to partial thermal-oxidative fragmentation of biocrude components into gas.58 In addition, repolymerization of components in lignin-derived biocrude into solid hydro-char may also occur due to faster decomposition of lignin-stabilizing agents (e.g., formaldehyde) above 330 °C.59

3.1.3 Effect of salt content. A higher salt content decreased the $Y_{\text{oil,daf}}$ (negative linear coefficient in Table 3). Salt in the digestate comprised mostly carbonate minerals (e.g., CaCO₃ and MgCO₃) and higher carbonate mineral concentrations may increase feedstock alkalinity (positive linear effect of salt content on ΔpH_{lig} , see Table 3) and direct cellulose and lignin decomposition toward the alkaline pathway. Alkaline-catalyzed retro-aldol condensation (r9), benzilic acid rearrangement (r10), and carbonyl cleavage (r11) convert cellulose into aqueous organics, such as lactic acid, acetaldehyde, acetic acid, and acetoin (see Table S8, ESI†), leading to a lower Yoil,daf. 55 Moreover, alkaline-catalyzed lignin degradation transformed phenolic units into quinone methides and non-phenolic units into phenyl-oxirane intermediates (r32),60,61 both of which are prone to condensation into hydro-char (r35 and r36).62 Enolethers (the products of retro-aldol decomposition of quinone methide, r33) and phenyl-oxiranes were present in the biocrudes produced from alkaline (pH 8.5) and high-salt-content (5 wt%) feedstocks (Table S10, ESI†). In addition, alkaline conditions also converted lignin into aqueous acetophenone and hydroxybenzoic acids (r30) according to Table S8 (ESI†).

3.1.4 Effect of cellulose-to-lignin ratio (Cel/Lig). The presence of more lignin in the digestate inhibited the biocrude formation (positive linear coefficient of Cel/Lig for Yoil.daf in Table 3). This inhibition may be associated with the susceptibility of lignin degradation products to recondensation into hydro-char.63 Despite previous studies reported restricted accessibility of cellulose due to lignin-cellulose complex formation for biomass waste as a cause for lower biocrude production,64 this is unlikely to be true for synthetic anaerobic digestates as lignin and cellulose were supplied as unbound pure components in the mixture. The negative effect lignin has on Yoil,daf can be mitigated by employing slightly less acidic feedstock pH (pH 4-5, see Fig. 2B) due to the positive interaction between feedstock pH and Cel/Lig (see Table 3).

3.2 Heteroatom content in biocrudes

3.2.1 Oxygen content. The oxygen content in the biocrudes (%O_{oil}) for all the experiments was 18.2-36.4% for DSO (dichloromethane-extracted solid-bound biocrude) and 29.7-43.7% for DWO (dichloromethane-extracted water-soluble biocrudes) - values higher than those in conventional crude oils.65 However, the regression models for %Ooil-DWO and %Ooil-DSO (see Table 3) revealed that the process conditions can be tailored to ensure HTL of anaerobic digestates produces biocrudes with the lowest possible oxygen content. High reaction temperatures and long reaction times decreased the oxygen content (see Fig. 2C), as indicated by the negative linear coefficients emphasizing negative interactions between factors (see Table 3). Specifically, reaction temperatures >310 °C and reaction times >30 min are recommended for feedstock with salt content >2 wt% and Cel/Lig > 1.2, respectively (Fig. 2D and E). Increasing the feedstock pH also significantly decreased the % $O_{\rm oil}$ with a plateau starting at pH \sim 6. For digestates containing Cel/Lig > 1.5, feedstock pH > 6 is not recommended because the oxygen content in biocrudes would slightly increase through the positive interaction of pH with Cel/Lig (Fig. 2F). These suggested process conditions were associated with decarboxylation (mostly in DSO) and dehydration (mostly in DWO) reactions, according to the Van Krevelen diagrams of different biocrude fractions shown in Fig. S13 and S14 (ESI†).

3.2.2 Nitrogen content. The nitrogen content in biocrudes obtained for all experiments varied between 2.1 and 5.4% for DWO and 1.0-3.1% for DSO. These levels exceed concentrations found in most conventional crude oil (0.25%).66 From the regression equations for %Noil-DWO and %Noil-DSO (see Table 3), feedstock pH was identified as the most important factor with a positive linear effect on biocrude nitrogen content (%Noil). This effect can be explained considering that at a higher feedstock pH (more alkaline), cellulose degradation proceeded mostly through the alkaline pathway and produced electrophilic α -dicarbonyl and α -hydroxycarbonyl compounds (e.g., glycolaldehyde, hydroxybutanone, methylglyoxal, and glyoxal (r9); see Table S8, ESI†), which are more reactive intermediates than reducing sugars for the Maillard reaction.⁶⁷ In addition, alkaline conditions increased the nucleophilicity of amino group of amino acids and ammonia, enhancing the Maillard reaction by forming aminocarbonyl intermediates through Strecker degradation of amino acids with the help of α-dicarbonyls (r14)68 and Amadori rearrangement of ammonia with α hydroxycarbonyls (r15).69 Pyridines, pyrazines, azoles, pyrroles, and their derivatives (see Table S7, ESI†) were observed as products of the Maillard reaction (aromagenic pathways),70,71 and the presence of amides (e.g., 9-octadecenamide and 13docosenamide) indicated that base-catalyzed ester aminolysis (r31) also contributed to nitrogen fixation in biocrude.⁷²

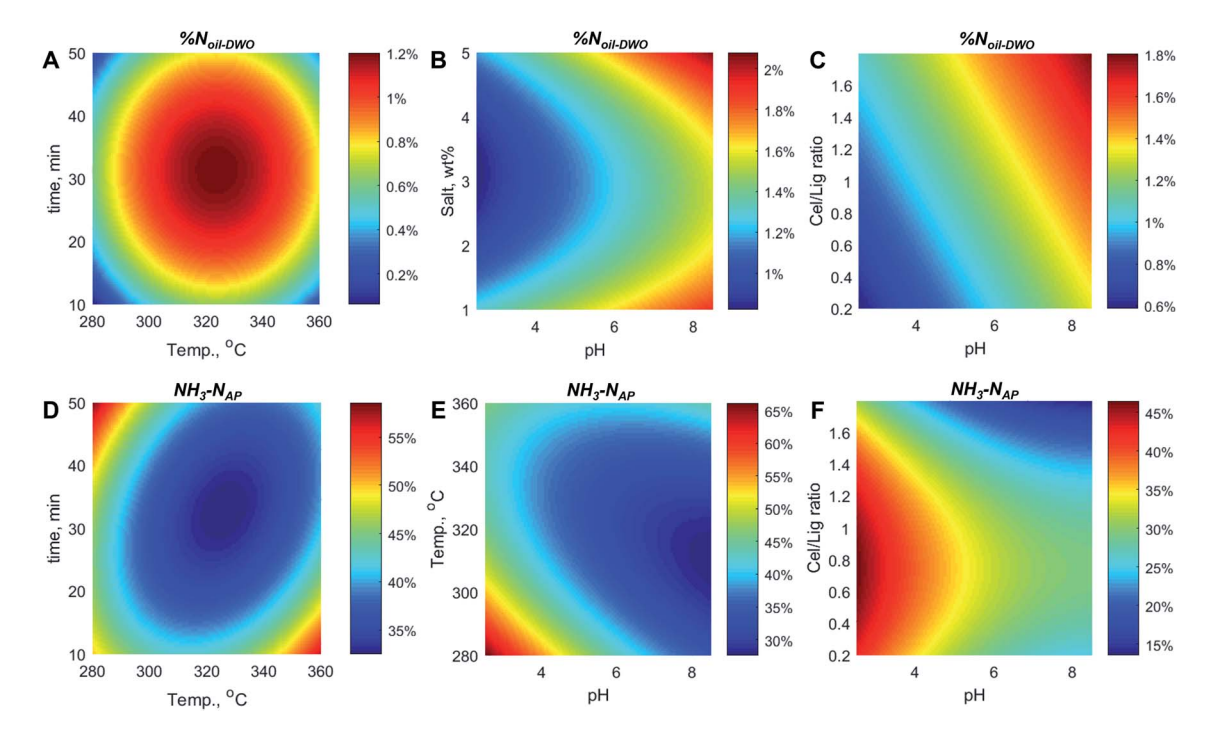
From the above explanations, low-pH feedstocks (acidic) can achieve lower $\%N_{\rm oil}$, because the Maillard reaction is inhibited. However, chemical compounds similar to Maillard reaction products, *i.e.*, caprolactam and pyrroles, still existed in biocrudes produced from acidic feedstocks (see Table S7, ESI†). Because the Maillard reaction is inhibited under acidic conditions, two potential alternative reaction mechanisms are Beckmann rearrangement (r28, cyclic C_6 -ketone conversion into caprolactam)⁷³ and Paal-Knorr condensation (r15, pyrrole formation from the reaction between 1,4-dicarbonyl compounds with amino-acid or ammonia),⁷⁴ both of which are acid-catalyzed. Detailed mechanisms have been described in the literature.^{73,74}

The $\%N_{\rm oil}$ showed quadratic dependence on reaction temperature and time (see Table 3), yielding global maxima at 330 $^{\circ}{\rm C}$ and 30 min (Fig. 3A). Therefore, lower temperatures coupled with shorter reaction times (milder conditions) and

higher temperatures coupled with longer reaction times (moresevere conditions) can produce low %Noil. The milder conditions decreased %Noil because reactions generating less polar N-heterocyclic compounds, such as the Maillard reaction, Paal-Knorr condensation, and ester aminolysis, were not fully activated under these conditions. Meanwhile, the higher temperatures and longer reaction times allowed the hydrodenitrogenation reaction to occur, removing nitrogen from biocrudes. The course of hydro-denitrogenation reactions in the high-severity process was demonstrated by an increase in peak area percentages of saturated heterocyclic amines, alkylamines, and alkanes in the biocrudes (see Table S7, ESI†). The increased detection of piperidines, piperazines, and pyrrolidines indicated the aromatic saturation (r16) of pyridines, pyrazines, and pyrroles, respectively. Aromatic saturation is critical to facilitate ring-opening (r17) by converting the hybridization state of carbons surrounding the C-N bond to sp3 to obtain a weaker bond dissociation energy. The increased detection of alkylamines and alkanes (C₄-C₅) indicated that the saturated aromatic rings of piperidine, piperazine, and pyrrolidine were opened via C-N bond cleavage, followed by deamination via Hoffmann elimination or S_N2-type substitution, releasing alkanes and NH₃ as a byproduct (r18).66,75,76

Increasing the feedstock cellulose-to-lignin ratio had a positive linear effect on %Noil (see Table 3 and Fig. 3C); in other words, a lower ratio, with higher lignin content than cellulose, suppressed nitrogen fixation in the biocrude. At lower Cel/Lig ratios, excess phenols or phenolic acids produced from the hydrothermal oxidative decomposition of lignin (r19) may prevent cellulose-derived α-dicarbonyls/α-hydroxycarbonyls from participating in nitrogen-fixing reactions (e.g., Maillard reaction and Paal-Knorr condensation). The potential prevention mechanism involves the capture of the electrophilic carbon of the carbonyl group by the aromatic rings of phenols or phenolic acid through an ortho- or para-directed electrophilic aromatic substitution (r20).77 Although products of this mechanism, such as dihydroxycinnamic-acid-2-glyoxal benzenetriol-2-butanedione, were not detected in biocrudes due to their non-volatile nature, several meta-hydroxyl-containing phenols (e.g., 3,5-dihydroxycinnamic acid, 1,3,5-benzenetriol, 5-tert-butylpyrogallol, and 3,5-dihydroxybenzoic acid) were detected with an increased extent in the HTL-AP of lignin-rich feedstock (see Table S8, ESI†). Since a meta configuration of the electron donor (-OH group) at carbons number 3 or 5 in the phenol ring has a higher reactivity toward carbonyl-capturing at the ortho or para position, their increased detection suggests that the capturing reaction (r20) is likely to occurr.⁷⁷

Salt content had a quadratic effect on the $\%N_{\rm oil}$ (see Table 3) with minima at 3 wt% (Fig. 3B). Thus, salt in the digestate both inhibited and promoted nitrogenous compound formation. A salt concentration of 1–3 wt% had an inhibiting effect on the % $N_{\rm oil}$ that might be associated with increasing divalent cation concentration identified by Topete-Betancourt *et al.*⁷⁸ as blocking agents in Maillard intermediate formation. A salt content of 3–5 wt% promoted nitrogenous compound formation due to the increased feedstock alkalinity, given that salts in the digestate are primarily carbonated salts.



Representative contour plots for biocrude nitrogen content (%N_{oil}) in DWO biocrude fractions (A-C) and NH₃-N yield in the HTL-AP (D-F).

The increasing feedstock alkalinity increased the feedstock pH and led to the formation of amides (r12 and r31) and Nheterocyclic compounds (r13 and r14) as indicated by compositional analysis of biocrudes from feedstock with a salt content of 5 wt% in Table S7 (ESI†).

3.3 Nutrient yield in the HTL-AP

3.3.1 NH₃-N. The NH₃-N yield in the HTL-AP (NH₃-N_{AP}) was between 18.21 and 52.03%, and was significantly correlated with the reaction temperature and time, feedstock pH, and the Cel/Lig ratio on NH₃-N_{AP} (see Table 3). The reaction temperature and time showed a positive quadratic correlation with global minima at 330 °C and 30 min, as illustrated in Fig. 3D. Fig. 3A and D show that the %Noil and NH3-NAP were inversely correlated; the opposite shapes of the contour plots (valleyshaped versus mountain-shaped) indicate similar operating conditions (330 °C and 30 min) for the global maxima and minima, respectively. This implies that a decrease in NH₃-N_{AP} was followed by an increase in %Noil, and vice versa, owing to nitrogen-fixing and nitrogen removal reactions that consumed and released NH3, respectively. In addition, a negative interaction between the reaction temperature and time (see Table 3) indicated that the highest NH₃-N_{AP} could be achieved by processing the digestates at 360 °C for 10 min or 280 °C for 50 min.

An expected inverse relationship between NH₃-N_{AP} and % Noil was also observed at different feedstock pH values. However, the positive interaction between the feedstock pH and reaction temperatures created a slightly different trend for NH₃- N_{AP} in the region of pH > 6 and temperature > 330 °C. The observed decreasing trend for NH3-NAP at pH 2.5-6 and reaction temperatures ≤330 °C (Fig. 3E) was replaced by a flat plateau indicating stabilized NH₃-N_{AP} at \sim 30-40%. The stabilized NH3-NAP may be associated with the hydrodenitrogenation of biocrudes at higher temperatures expelling a sufficient amount of nitrogen as NH3-N to offset the amount of NH3-N fixed into biocrudes. The mechanism of hydrodenitrogenation is discussed in subsection 3.2.2.

For different Cel/Lig ratios, no inverse relationship between NH₃-N_{AP} and %N_{oil} was observed: the Cel/Lig ratio showed a negative quadratic effect (instead of a negative linear effect) on NH_3-N_{AP} with maxima at 0.75 (see Table 3 and Fig. 3F). The decrease in NH₃-N_{AP} with a Cel/Lig ratio decrease from 0.75 to 0.2 indicated that although nitrogen fixation into biocrude was inhibited at lower Cel/Lig ratios (sub-section 3.2.2), NH₃-N was still consumed by lignin decomposition products, generating aqueous-phase nitrogenous products. NH3-N may react with lignin-derived phenols and carboxylic acids, thus producing amines (e.g., 4-aminophenol, 2,6-dimethylaniline, and benzidine) and amides (e.g., dimethylbenzamide, acetamide, and methacrylamide), respectively (see Table S8, ESI†), via condensation reactions (r26 and r12).79-81

3.3.2 Phosphorus (P). The phosphorus yield in the HTL-AP (PAP) obtained from HFCCD experiments was 4.94-77.02%. Feedstock pH was the most statistically significant factor with a quadratic relationship (see Table 3), exhibiting minima at pH \sim 6 (Fig. 4B). The quadratic relationship between P_{AP} and feedstock pH showed the same trend as the pH-dependent solubility isotherm of brushite (CaHPO4·2H2O) in the Ca(OH)₂-H₃PO₄-H₂O ternary system and Ca(OH)₂-H₃PO₄-HCl-H₂O quaternary system.⁸² This similarity was expected because phosphorus in the digestate existed mostly as brushite, thus revealing two primary mechanisms accounting for the PAP increase at more acidic and more alkaline feedstock pH.

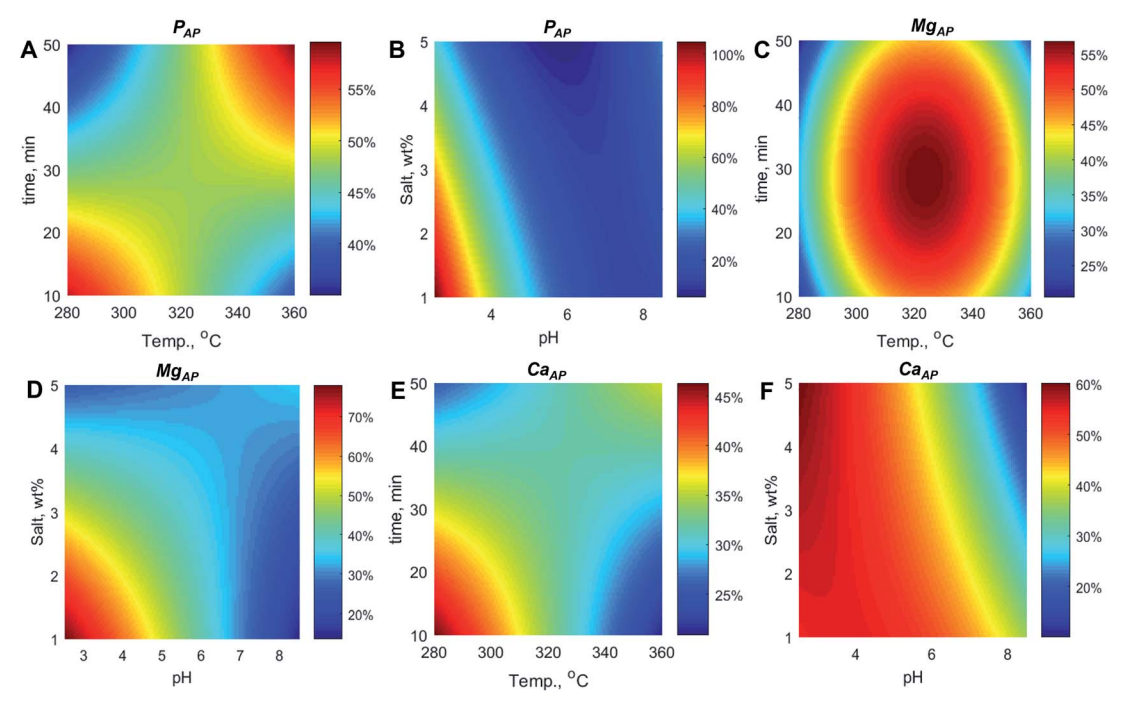
First, phosphorus from more acidic feedstock was increasingly partitioned into the HTL-AP because phosphate minerals are more soluble at lower pH (r48). Secondly, the observed increase of PAP at feedstock pH > 6 was associated with H3PO4 release into the HTL-AP after brushite hydrolysis (r46 and r47) into the more thermodynamically stable hydroxyapatite (Ca₁₀(PO₄)₆OH₂) and whitlockite (Ca₉MgHPO₄(PO₄)₆).83 The hydrolysis of brushite occurred at alkaline pH because hydroxyapatite and whitlockite were observed only in the hydro-char produced from the alkaline feedstock (pH 8.5, see Fig. S15E, ESI†), but they were not detected in the hydro-char produced from the acidic feedstock (see Fig. S15D, ESI†).

The second and the third most important factors for PAP were salt content and the Cel/Lig ratio. The salt content was negatively correlated with PAP. Higher salt content may increase the reaction medium alkalinity, as demonstrated by the positive linear effect of salt content on ΔpH_{liq} (see Table 3). Consequently, phosphate mineral solubility decreased, and PAP decreased. In addition, a positive interaction was observed between the salt content and feedstock pH (see Table 3); thus, PAP slightly increased with increasing salt content in alkaline feedstock (Fig. 4B). However, increasing the Cel/Lig ratio in the feedstock yielded more phosphorus in the HTL-AP because cellulose degradation through the acidic or alkaline pathway produced acids as side products, dissolving phosphate minerals. The acid production was confirmed by the negative linear effect of the Cel/Lig ratio on ΔpH_{liq} (see Table 3). However, a slight PAP decrease was observed with increasing Cel/Lig ratio in the alkaline feedstock (see Fig. S10, ESI†), due to the negative interaction between the Cel/Lig ratio and feedstock pH (see Table 3). A negative interaction was also observed between the Cel/Lig ratio and salt content, thus resulting in

a lower increase in PAP with the Cel/Lig ratio at higher salt content (see Fig. S10, ESI†).

The effects of reaction temperature and time were less significant than the other factors, as indicated by the smaller values of their respective linear coefficients and their interaction term coefficient in Table 3. Nevertheless, the observed positive interaction between those two factors revealed that higher PAP could be achieved with HTL under more severe conditions (Fig. 4A), under which the ability to extract more phosphorus into the HTL-AP was attributed to the enhanced acid production, as demonstrated by the coefficients of the linear and interaction terms of reaction temperature and time in the ΔpH_{lig} model (see Table 3).

3.3.3 Calcium (Ca) and magnesium (Mg). The yield of calcium and magnesium in the HTL-AP (CaAP and MgAP) was 11.24-56.01% and 5.43-93.68%, respectively. Both CaAP and Mg_{AP} decreased significantly when the feedstock pH increased (see Table 3, Fig. 4D and F), because the solubility of calcium and magnesium minerals was negatively correlated with pH. Similarly, higher salt content produced lower CaAP and MgAP because the increased alkalinity in the digestate from the presence of more carbonate salts may retain calcium and magnesium in the solid phase as calcite (a trigonal-structured polymorph of CaCO₃, r38), lansfordite (MgCO₃·5H₂O, r40), and hydromagnesite (Mg₅(CO₃)₄(OH)₂·4H₂O, r43), as shown in Fig. S15 (ESI†). However, the Mg_{AP} decrease at higher salt content was observed only at feedstock pH \leq 6.5 due to the positive interaction between the feedstock pH and salt content (see Table 3). At feedstock pH > 6.5, Mg_{AP} was relatively constant at \sim 25% at any feedstock salt content (see Fig. S12, ESI†). Meanwhile, the observed negative interaction between the feedstock pH and salt content in the CaAP model (see Table 3)



Representative contour plots of nutrient yield in the HTL-AP: phosphorus (A and B), magnesium (C and D), and calcium (E and F).

resulted in a steeper decrease in Ca_{AP} at higher feedstock pH and salt contents.

The Cel/Lig ratio had a statistically significant effect on only Ca_{AP} (see Table 3). Higher Cel/Lig ratios linearly increased Ca_{AP} because higher cellulose content enabled the production of more acids, which decreased the pH and increased the solubility of calcium minerals. Nevertheless, because of the negative relationship between the salt content and Cel/Lig ratio, the Ca_{AP} increase gradually disappeared at higher feedstock salt content. A feedstock salt content of 4 wt% was the inflection point of the slope of Ca_{AP} . Thus, higher Cel/Lig ratios in high-salinity feedstock (>4 wt%) resulted in lower Ca_{AP} because carbonate salts may provide a high buffering capacity that resists the decrease in reaction medium pH.

The HTL operating conditions showed different effects on Ca_{AP} and Mg_{AP}. Increasing the reaction temperature at reaction times ≤35 min decreased Ca_{AP} (Fig. 4E), in accordance with the solubility of calcium minerals, such as CaCO₃, that is negatively correlated with temperature. However, CaAP increased at higher temperatures and a reaction time > 35 min. The mechanisms underlying these findings may be associated with the phase transition of less soluble to more soluble calcium minerals. The dominating polymorphs of CaCO₃ were aragonite and vaterite in the hydro-char produced from more-severe conditions (see Fig. S15C, ESI†). In contrast, calcite was the only detected CaCO₃ polymorph in the hydro-char produced from less-severe conditions (see Fig. S15A, D and E, ESI†). Aragonite and vaterite are orthorhombic and hexagonal polymorphs of CaCO₃, respectively, which are more soluble than calcite (trigonalstructured). Because aragonite is the most stable phase of CaCO₃ under high pressure, more-severe conditions (including higher pressures) can induce the phase transformation of calcite into aragonite (r37).84 Meanwhile, the establishment and stabilization of vaterite under more severe conditions was promoted by increased production of hydrophilic organic macromolecules (r39), e.g., phenols, aldehydes, and ketones, 85 which may create hydrogen-bonded networks with water and deplete free H2O molecules. Consequently, the initially formed vaterite crystals did not readily transform into calcite and continued to aggregate and precipitate, forming more vaterites.86

The reaction temperature and time had quadratic effects on Mg_{AP} (see Table 3), yielding global maxima at 320 °C and 30 min, respectively (Fig. 4C). Mg_{AP} increased at 280–320 $^{\circ}\text{C}$ because magnesium in hydro-char existed mostly as lansfordite (MgCO₃·5H₂O, see Fig. S15A, ESI†), whose solubility increases with temperature.87 At temperatures >320 °C, nesquehonite (MgCO₃·3H₂O) was the primary magnesium mineral in the hydro-char (see Fig. S15B, ESI†). This suggests that lansfordite was dehydrated into nesquehonite (r41). Because the solubility of nesquehonite decreases with temperature, 87 at >320 $^{\circ}$ C, Mg_{AP} decreased. At a reaction time >30 min, more-hydrated magnesium carbonates were dehydrated (r41 and r42); in addition, nesquehonite formation at 280-320 °C (after previous production of mostly lansfordite at reaction times <30 min) and magnesite (anhydrous MgCO₃) formation at 320-360 °C (after the previous production of mostly nesquehonite at reaction

time <30 min) were enhanced (see Fig. S15A–C, ESI†). The formation of less-hydrated Mg-carbonates at a reaction time >30 min may explain the Mg_{AP} decrease at 30–50 min because less-hydrated phases were less soluble than the more-hydrated phases.⁸⁷

4. Optimization and validation of HTL operating conditions

This section describes the multi-objective optimization and presents the optimal ranges of reaction temperature, reaction time, and feedstock pH leading to maximum energy and nutrient recoveries based on the different feedstock compositions. The validation of the optimization results is also presented.

The optimal conditions to achieve the optimization objectives were achieved over the range of Cel/Lig ratios and salt contents studied (see Fig. 5). The composite desirability and the values of optimized responses under these optimal conditions are given in Fig. S16 and S17 (ESI†). In general, an initial feedstock pH of ~ 3.00 –3.90 is suitable for processing digestates containing salt <4 wt% (Fig. 5C). Acidic conditions increased the biocrude production and nutrient yield in the HTL-AP and inhibited the nitrogen fixation in biocrude and the recondensation of oily lignin monomers into hydro-char. However, at a salt content ≥ 4 wt%, a less acidic pH for the digestate (3.91–5.53) and HTL operation at 343–354 °C are recommended (Fig. 5A).

According to the desirability plots (see Fig. S18, ESI†), higher salt content decreased the individual desirability of biocrude yield, ER $_{\rm oil}$, PAP, and %N $_{\rm oil}$. Adjusting the digestate pH to \sim 3.91–5.53 may improve the individual desirability of biocrude yield and ER $_{\rm oil}$, because a feedstock pH of \sim 4–5.5 provided the highest biocrude yield and energy recovery (see sub-section 3.1.1). Moreover, the improvements in PAP and %N $_{\rm oil}$ were achieved by increasing the reaction temperature to 354 °C to promote partial removal of nitrogen from biocrude as NH $_{\rm 3}$ –N via HDN reactions (see sub-section 3.2.2) and to enhance phosphorus mineral dissolution in the HTL-AP through acid production (see sub-section 3.3.2).

Similarly, higher reaction temperatures up to 360 °C were required by cellulose-rich digestates (Cel/Lig > 1, Fig. 5A) to expel nitrogen fixed by cellulose-derived carbonyl compounds into the biocrude (see sub-section 3.2.2 for the denitrogenation mechanism). Combined with shorter reaction times, as suggested in Fig. 5B, the lowest %Noil was 0.14–0.21% (see Fig. S17, ESI†). Meanwhile, a reaction time of 45–50 min and a reaction temperature of 337–358 °C were required by lignin-rich digestates (Cel/Lig < 1) to compensate for the adverse effects of higher lignin content (see Fig. S18, ESI†), *i.e.*, lower ERoil, lower PAP, and higher %Ooil.

The optimum HTL operating conditions were confirmed through a five-time-replicated experimental validation test on digestates with four different compositions: (1) salt 2 wt% and Cel/Lig 0.4; (2) salt 2 wt% and Cel/Lig 1.6; (3) salt 4 wt% and Cel/Lig 0.4; and (4) salt 4 wt% and Cel/Lig 1.6. The small differences



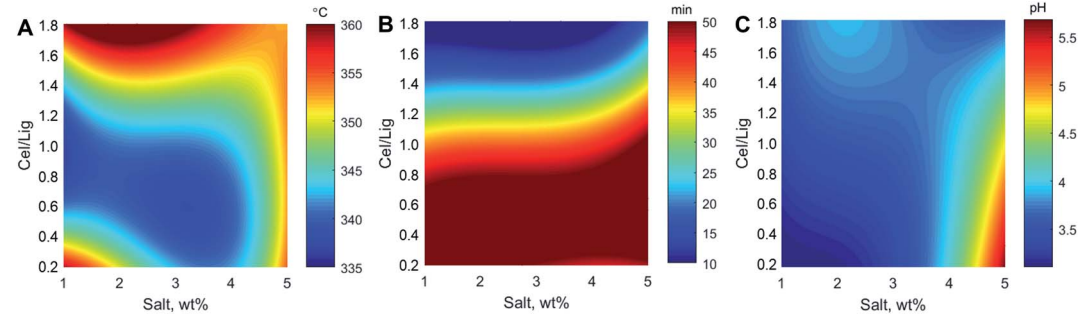


Fig. 5 Contour plots of optimal (A) reaction temperature, (B) reaction time, and (C) feedstock pH for processing digestates with cellulose-tolignin ratio (Cel/Lig) 0.2-1.8 and salt content 1-5 wt%

Table 4 Validation results for multi-objective optimization. Pred. = predicted value; Exp. = experimental value; and Diff. = difference between Pred. and the average value of Exp

	Digestate 1 Salt: 2 wt% Cel/Lig: 0.4 T: 348.7 °C t: 50 min pH: 3.23			Digestate 2 Salt: 2 wt% Cel/Lig: 1.6 T: 359.2 °C t: 10 min pH: 3.53			Digestate 3 Salt: 4 wt% Cel/Lig: 0.4 T: 339.6 °C t: 50 min pH: 3.77			Digestate 4 Salt: 4 wt% Cel/Lig: 1.6 T: 354.3 °C t: 10 min pH: 3.77		
Optimized				Pred.			Pred.			Pred.		
responses	Pred. (%)	Exp. (%)	Diff. (%)	(%)	Exp. (%)	Diff. (%)	(%)	Exp. (%)	Diff. (%)	(%)	Exp. (%)	Diff. (%)
$Y_{\rm oil,daf}$	42.7	42.6 ± 0.2	0.1	42.4	42.6 ± 0.4	-0.2	36.0	35.4 ± 0.6	0.6	34.9	35.2 ± 0.1	-0.3
ER_{oil}	63.4	63.2 ± 0.3	0.2	71.0	$\textbf{70.4} \pm \textbf{0.6}$	0.6	61.7	$\textbf{61.8} \pm \textbf{0.3}$	-0.1	66.0	65.5 ± 0.5	0.5
$\rm \%O_{DWO}$	32.8	32.9 ± 0.3	-0.1	38.9	39.4 ± 0.6	-0.5	32.4	32.1 ± 0.4	0.3	37.0	37.0 ± 0.3	0.0
$\rm ^{\!\! MO_{DSO}}$	23.6	24.0 ± 0.5	-0.4	25.3	25.9 ± 0.3	-0.6	17.4	17.4 ± 0.5	0.0	22.2	22.5 ± 0.2	-0.3
$%N_{DWO}$	0.4	0.4 ± 0.1	0.0	0.0	0.1 ± 0.0	0.0	1.2	1.1 ± 0.1	0.1	0.3	0.2 ± 0.3	0.1
$%N_{DSO}$	0.1	0.1 ± 0.1	0.0	0.3	0.4 ± 0.1	-0.1	0.4	0.4 ± 0.1	0.0	0.5	0.6 ± 0.0	-0.1
P_{AP}	49.6	49.2 ± 0.3	0.4	74.8	74.2 ± 0.4	0.6	24.8	25.3 ± 0.6	-0.5	33.7	33.6 ± 0.3	0.1
NH_3-N_{AP}	46.5	46.4 ± 0.2	0.1	52.0	52.3 ± 0.6	-0.3	44.7	44.9 ± 0.4	-0.2	49.2	48.9 ± 0.4	0.3
Mg_{AP}	75.2	75.3 ± 0.5	-0.1	65.3	64.6 ± 0.7	0.7	68.1	67.6 ± 0.4	0.5	61.4	$\textbf{61.7} \pm \textbf{0.4}$	-0.3
Ca _{AP}	36.3	$\textbf{36.1} \pm \textbf{1.0}$	0.2	36.2	37.6 ± 0.1	-1.4	40.7	40.7 ± 0.9	0.0	30.3	$\textbf{29.9} \pm \textbf{0.4}$	0.4

between the predicted and experimental values of all optimized responses (see Table 4) demonstrate the response models' validity and accuracy for all investigated combinations of independent variables.

Summary of experimentally validated reaction pathways under optimized conditions

In summary, under optimized HTL process conditions (e.g., acidic feedstock pH), the biocrude oil is produced from cellulose and lignin conversion into cyclic (C₅- and C₆-) ketones (r7), alkylfurans (r8), alkyl-methoxyphenols (r29), C2-aldehyde-susbtituted phenols (r21), benzodioxanes (r25), benzodioxolanes (r23), and benzopyrans (r22). However, cellulose is also converted into soluble compounds that partition in the AP, for example from acid-catalyzed retro-aldol condensation (r9) of carbohydrate

monomers (e.g., α-hydroxycarbonyls, α-dicarbonyls, acids, and aldehydes) and acid-catalyzed rehydration (r3) of 5-HMF (i.e., levulinic acid and formic acid), while lignin acidolysis (r21) produces aqueous-phase organics such as phenols, hydroxyphenols, phenolic acids (r19), and aromatic amines (r26). In addition, acidic feedstock pH enhances nitrogen fixation in the biocrude through the Paal-Knorr condensation reaction (r15) between α-dicarbonyls and NH₃ or amino acid to form pyrroles, and through Beckmann rearrangement (r28) of phenol-derived cyclic C₆-ketones into caprolactam. Processing the digestates at high reaction temperatures and long processing times removes nitrogen from biocrude as NH3-N through hydrodenitrogenation, by converting N-heterocyclic compounds into aliphatic alkanes through aromatic-ring saturation (r16) and opening (r17) and alkylamine deamination (r18). The low pH also partitions most of the Mg and P into AP by enhancing their solubilities (r48 and r49), while Ca mostly precipitates in the

hydrochar as calcite (r38), aragonite (r37), and vaterite (r39), due to its lower solubility compared to Mg and P minerals.

Conclusions and recommendations

An experimental study of hydrothermal liquefaction (HTL) of selected model anaerobic digestates representative of dairy waste feedstocks was conducted. A comprehensive HTL reaction pathway for anaerobic digestates was proposed based on interpretations of the statistical analysis results of our experimental study and their comparison with the available published results from earlier studies. A range of waste compositions and experimental conditions were used: HTL temperature of 280-360 °C, reaction time of 10-50 min, feedstock pH of 2.5-8.5, digestate salt content of 1-5 wt%, and digestate cellulose-to-lignin ratio of 0.2-1.8. Thirty-two HTL experiments were conducted following a response surface design methodology based on a half-fractional central composite design. The HTL products of each run were analyzed using elemental analysis, GC-MS, XRD, and colorimetric techniques. Using the results from these analyses, quadratic regression equations for each response variable were obtained. Subsequently in analyzing the data, a desirability function approach was used to specify the HTL conditions that simultaneously maximize the biocrude energy recovery, minimize the biocrude heteroatom content, and maximize the nutrient yield (i.e., NH₃-N, Mg, and P) in the aqueous-phase coproduct for the different digestate compositions. Additional HTL experiments validated this optimization method and its accuracy.

The optimization results uncover the mechanistic significance of pre-acidifying the feedstock (pH 3.00-5.53) using acetic acid and processing at high reaction temperatures (337–360 °C) and over a broad range of reaction times (10-50 min) depending on the cellulose-to-lignin ratio for maximum biocrude energy recovery and nutrient yield in the HTL-AP. Under such conditions, the biocrude yield is maximized as cellulose is converted into pyrones, cyclic ketones, furanones, and aliphatic alkanes while lignin into alkyl-substituted methoxyphenols, hydroxymethylated phenols, dioxanes/dioxolanes, and pyrans. Moreover, the Maillard reaction (responsible for the formation of Ncontaining α -dicarbonyls and α -hydroxycarbonyls in the oil) is inhibited, and deoxygenation and hydro-denitrogenation contribute to minimizing the biocrude heteroatom content. Nutrients (i.e., NH3-N, P, and Mg) are effectively partitioned in the aqueous phase as acidic conditions prevent them from precipitating as hydroxyapatite, whitlockite, or MgCO₃ minerals in the hydrochar. The only exception is Ca, which effectively precipitates as calcite in the solid hydrochar phase.

The nutrients partitioned into the aqueous phase product (HTL-AP) will need to be recovered ultimately to demonstrate economic viability with a more sustainable outcome, consistent with achieving a circular bioeconomy. A possible pathway for the recovery of both N and P is to crystallize struvite from the HTL aqueous phase. Future studies are required to describe and optimize the struvite crystallization process from actual wastewater. This topic will be the target of a future publication. In

addition, while this work demonstrates the possibility of simultaneously optimizing both energy recovery in biocrude and nutrient yield in the aqueous phase coproduct, the determined optimal HTL operating conditions require high temperatures and large quantities of acetic acid to control the feedstock pH, which may not be economically viable. Future research should therefore identify alternatives to acetic acid (i.e., other inexpensive organic acids, or heterogeneous solid acid catalysts) that can maximize energy and nutrient recovery for digestates using HTL under milder operating conditions to lower the operational cost of HTL.

Conflicts of interest

The authors declare no conflicts of interest to disclose.

Author contributions

Hanifrahmawan Sudibyo: conceptualization, methodology, formal analysis, investigation, data curation, visualization, and writing - original draft. Matteo Pecchi: conceptualization, formal analysis, visualization, and writing - review & editing. Jefferson William Tester: conceptualization, methodology, writing - review & editing, supervision, and funding acquisition.

Acknowledgements

This study was funded in part by the Cornell Energy Systems Institute, the Graduate School at Cornell, the U.S. Department of Energy (DOE) through their RAPID program, and the USDA grant 2019-69012-29905 that involves collaborative research between Cornell University and the University of Arkansas. This study also utilized the Cornell Center for Materials Research Shared Facilities (NSF MRSEC DMR-1719875). The authors thank Dr Kui Wang for providing technical assistance during the experimental work performed as part of this study. The first author also thanks the Fulbright-DIKTI Foundation for support through a doctoral fellowship in chemical engineering at Cornell University.

References

- 1 NCBA, Beef Industry Overview, https://www.ncba.org/ producers/industry-statistics, accessed May 16, 2021.
- 2 United States Environmental Protection Agency, 2018 Wasted Food Report, Washington D.C., 2020.
- 3 H. Sudibyo, Z. L. Shabrina, L. Halim and W. Budhijanto, Energy Procedia, 2017, 105, 256-262.
- 4 R. Nkoa, Agron. Sustainable Dev., 2014, 34, 473-492.
- 5 Zeshan and C. Visvanathan, Int. Biodeterior. Biodegrad., 2014, 95, 167-175.
- 6 G. A. Iocoli, M. C. Zabaloy, G. Pasdevicelli and M. A. Gómez, Sci. Total Environ., 2019, 647, 11-19.
- 7 C. Le Maréchal, C. Druilhe, E. Repérant, E. Boscher, S. Rouxel, S. Le Roux, T. Poëzévara, C. Ziebal, C. Houdayer, B. Nagard, F. Barbut, A. M. Pourcher and M. Denis, MicrobiologyOpen, 2019, 8, 1-10.

- 8 W. Wang and D. J. Lee, Bioresour. Technol., 2021, 323, 124626.
- 9 A. A. Peterson, F. Vogel, R. P. Lachance, M. Fröling, M. J. Antal and J. W. Tester, Energy Environ. Sci., 2008, 1,
- 10 M. Pecchi and M. Baratieri, Renewable Sustainable Energy Rev., 2019, 105, 462-475.
- 11 Y. Fan, U. Hornung, N. Dahmen and A. Kruse, Biomass Convers. Biorefin., 2018, 8, 909-923.
- 12 R. Posmanik, D. A. Cantero, A. Malkani, D. L. Sills and J. W. Tester, J. Supercrit. Fluids, 2017, 119, 26-35.
- 13 R. Obeid, D. M. Lewis, N. Smith, T. Hall and P. van Eyk, Chem. Eng. J., 2020, 389, 1-14.
- 14 J. Yang, Q. He, K. Corscadden, H. Niu, J. Lin and T. Astatkie, Appl. Energy, 2019, 233-234, 906-915.
- 15 T. Yang, Y. Jie, B. Li, X. Kai, Z. Yan and R. Li, Fuel Process. Technol., 2016, 148, 19-27.
- 16 F. Cheng, G. A. Tompsett, D. V. Fraga Alvarez, C. I. Romo, A. M. McKenna, S. F. Niles, R. K. Nelson, C. M. Reddy, S. Granados-Fócil, A. D. Paulsen, R. Zhang and M. T. Timko, Sustainable Energy Fuels, 2021, 5, 941-955.
- 17 R. Posmanik, C. M. Martinez, B. Cantero-Tubilla, D. A. Cantero, D. L. Sills, M. J. Cocero and J. W. Tester, ACS Sustainable Chem. Eng., 2018, 6, 2724-2732.
- 18 X. Zhang, K. Wilson and A. F. Lee, Chem. Rev., 2016, 116, 12328-12368.
- 19 B. M. Ghanim, W. Kwapinski and J. J. Leahy, ACS Sustainable Chem. Eng., 2018, 6, 11265-11272.
- 20 H. Sudibyo, K. Wang and J. W. Tester, ACS Sustainable Chem. Eng., 2021, 9, 11403-11415.
- 21 Q. Wang, H. Jung, B. Wan, P. Liu, P. Yang and Y. Tang, ACS Sustainable Chem. Eng., 2021, 9, 10630-10641.
- 22 D. Crutchik and J. M. Garrido, *Chemosphere*, 2016, **154**, 567– 572.
- 23 U. Ekpo, A. B. Ross, M. A. Camargo-Valero and P. T. Williams, Bioresour. Technol., 2016, 200, 951-960.
- 24 U. Ekpo, A. B. Ross, M. A. Camargo-Valero and L. A. Fletcher, Bioresour. Technol., 2016, 214, 637-644.
- 25 N. R. Costa, J. Lourenço and Z. L. Pereira, Chemom. Intell. Lab. Syst., 2011, 107, 234-244.
- 26 K. Möller and T. Müller, Eng. Life Sci., 2012, 12, 242-257.
- 27 Y. Zhong, Z. Liu, C. Isaguirre, Y. Liu and W. Liao, Biotechnol. Biofuels, 2016, 9, 1-11.
- 28 K. Risberg, H. Cederlund, M. Pell, V. Arthurson and A. Schnürer, Waste Manag., 2017, 61, 529-538.
- 29 K. Güngör and K. G. Karthikeyan, Bioresour. Technol., 2008, 99, 425-436.
- 30 W. Tao, K. P. Fattah and M. P. Huchzermeier, J. Environ. Manage., 2016, 169, 46-57.
- 31 American Society for Testing and Materials (ASTM), ASTM E1131-20 Standard Test Method for Compositional Analysis by Thermogravimetry, West Conshohocken, Pennsylvania, 2015, vol. 8.
- 32 S. A. Channiwala and P. P. Parikh, Fuel, 2002, 81, 1051-1063.
- 33 American Society for Testing and Materials (ASTM), ASTM D1426-15 Standard Test Methods for Ammonia Nitrogen In Water, United States, 2015.

- 34 APHA (American Public Health Association), Standard Methods for the Examination of Water and Wastewater, APHA (American Public Health Association), Washington D.C., 20th edn, 1999.
- 35 K. S. Crane, B. L. Webb, P. S. Allen and V. D. Jolley, Commun. Soil Sci. Plant Anal., 2005, 36, 2687-2697.
- 36 Environmental Protection Agency (EPA), in Test Methods for Evaluating Solid Waste, Physical/Chemical Methods SW-846, Environmental Protection Agency (EPA), Washington D.C., 3rd edn, 2015, pp. 1-5.
- 37 M. F. Ryan and H. Barbour, Ann. Clin. Biochem., 1998, 35, 449-459.
- 38 R. W. Wells, Am. J. Clin. Pathol., 1948, 18, 576-578.
- 39 R. B. Madsen, M. M. Jensen, A. J. Mørup, K. Houlberg, P. S. Christensen, M. Klemmer, J. Becker, B. B. Iversen and M. Glasius, Anal. Bioanal. Chem., 2016, 408, 2171-2183.
- 40 D. C. Montgomery and G. C. Runger, in Applied Statistics and Probability for Engineers, John Wiley and Sons, Inc., New York, NY, 3rd edn, 2002, p. subsection 14-10.
- 41 C. Yang, S. Wang, J. Yang, D. Xu, Y. Li, J. Li and Y. Zhang, Green Chem., 2020, 22, 8210-8232.
- 42 W. Schutyser, T. Renders, S. Van Den Bosch, S. F. Koelewijn, G. T. Beckham and B. F. Sels, Chem. Soc. Rev., 2018, 47, 852-908.
- 43 J. Yang, Q. He, K. Corscadden, H. Niu, J. Lin and T. Astatkie, Appl. Energy, 2019, 233-234, 906-915.
- 44 M. H. Marzbali, S. Kundu, P. Halder, S. Patel, I. G. Hakeem, J. Paz-Ferreiro, S. Madapusi, A. Surapaneni and K. Shah, Chemosphere, 2021, 279, 130557.
- 45 T. Shen, R. Hu, C. Zhu, M. Li, W. Zhuang, C. Tang and H. Ying, RSC Adv., 2018, 8, 37993-38001.
- 46 S. Al-Hammadi and G. da Silva, Phys. Chem. Chem. Phys., 2021, 23, 2046-2054.
- 47 M. Chatterjee, T. Ishizaka and H. Kawanami, Green Chem., 2018, 20, 2345-2355.
- 48 J. N. M. Tan-Soetedjo, H. H. Van De Bovenkamp, R. M. Abdilla, C. B. Rasrendra, J. Van Ginkel and H. J. Heeres, Ind. Eng. Chem. Res., 2017, 56, 13228-13239.
- 49 F. Jin and H. Enomoto, Energy Environ. Sci., 2011, 4, 382-397.
- 50 M. R. Sturgeon, S. Kim, K. Lawrence, R. S. Paton, S. C. Chmely, M. Nimlos, T. D. Foust and G. T. Beckham, ACS Sustainable Chem. Eng., 2014, 2, 472-485.
- 51 S. Huang, N. Mahmood, M. Tymchyshyn, Z. Yuan and C. C. Xu, Bioresour. Technol., 2014, 171, 95-102.
- 52 S. Liu, J. Han, Q. Wu, B. Bian, L. Li, S. Yu, J. Song, C. Zhang and A. J. Ragauskas, Catal. Lett., 2019, 149, 2383-2389.
- 53 L. Shuai and B. Saha, Green Chem., 2017, 19, 3752-3758.
- 54 L. Shuai, M. T. Amiri, Y. M. Questell-Santiago, F. Héroguel, Y. Li, H. Kim, R. Meilan, C. Chapple, J. Ralph and J. S. Luterbacher, Science, 2016, 354, 329-333.
- 55 Z. Srokol, A. G. Bouche, A. Van Estrik, R. C. J. Strik, T. Maschmeyer and J. A. Peters, Carbohydr. Res., 2004, 339, 1717-1726.
- 56 Z. Wang, in Comprehensive Organic Name Reactions and Reagents, John Wiley & Sons, Inc., 2010, pp. 982–985.
- 57 W. Wang, Y. Liu, Z. Liu and S. Tian, Energy Fuels, 2016, 30, 968-974.

- 58 M. N. Islam, G. Taki, M. Rana and J. H. Park, Ind. Eng. Chem. Res., 2018, 57, 4779-4784.
- 59 H. Pińkowska, P. Wolak and A. Złocińska, Chem. Eng. J., 2012, 187, 410-414.
- 60 F. S. Chakar and A. J. Ragauskas, Ind. Crops Prod., 2004, 20, 131-141.
- 61 C. Lapierre, in Lignin and Lignans: Advances in Chemistry, ed. C. Heitner, D. Dimmel and J. Schmidt, Boca Raton, 1st edn, 2010, pp. 11-48.
- 62 S. Kang, X. Li, J. Fan and J. Chang, Renewable Sustainable Energy Rev., 2013, 27, 546-558.
- 63 E. Nagel and C. Zhang, Ind. Eng. Chem. Res., 2019, 58, 18866-18880.
- 64 M. Li, Y. Pu and A. J. Ragauskas, Front. Chem., 2016, 4, 1-8.
- 65 Environmental Protection Agency (EPA), Consolidated List of Reformulated Gasoline and Anti-Dumping Questions and Answers, Washington D.C., 2003.
- 66 G. H. C. Prado, Y. Rao and A. De Klerk, Energy Fuels, 2017, 31, 14-36.
- 67 A. A. Peterson, R. P. Lachance and J. W. Tester, Ind. Eng. Chem. Res., 2010, 49, 2107-2117.
- 68 Q. Zhang, J. M. Ames, R. D. Smith, J. W. Baynes and T. O. Metz, J. Proteome Res., 2009, 8, 754-769.
- 69 V. A. Yaylayan, Food Sci. Technol. Res., 2003, 9, 1-6.
- 70 X. Wu, M. Huang, F. Kong and S. Yu, J. Dairy Sci., 2015, 98, 8565-8571.
- 71 A. N. Yu, Z. W. Tan and F. S. Wang, LWT-Food Sci. Technol., 2013, 50, 64-71,
- 72 Y. S. Bao, B. Zhaorigetu, B. Agula, M. Baiyin and M. Jia, J. Org. Chem., 2014, 79, 803-808.
- 73 R. Mocci, E. Colacino, L. De Luca, C. Fattuoni, A. Porcheddu and F. Delogu, ACS Sustainable Chem. Eng., 2021, 9, 2100-2114.

- 74 L. Zhang, J. Zhang, J. Ma, D. J. Cheng and B. Tan, J. Am. Chem. Soc., 2017, 139, 1714-1717.
- 75 C. S. Raghuveer, J. W. Thybaut, R. De Bruycker, K. Metaxas, T. Bera and G. B. Marin, Fuel, 2014, 125, 206-218.
- 76 Y. Guo, X. Liu, P. Duan, D. Xu and R. Luque, ACS Sustainable Chem. Eng., 2021, 9, 362-374.
- 77 B. de Falco, A. Petridis, P. Paramasivan, A. D. Troise, A. Scaloni, Y. Deeni, W. E. Stephens and A. Fiore, RSC Adv., 2020, 10, 21535-21544.
- 78 A. Topete-Betancourt, J. d. D. Figueroa Cárdenas, A. L. Rodríguez-Lino, E. Ríos-Leal, E. Morales-Sánchez and H. E. Martínez-Flores, Food Sci. Biotechnol., 2019, 28, 975-982.
- 79 S. Bugosen, I. D. Mantilla and F. Tarazona-Vasquez, Heliyon, 2020, 6, e05778.
- 80 V. V. Bochkarev, L. S. Soroka, T. A. Klimova and L. E. Velikorechina, *Procedia Chem.*, 2015, **15**, 320–325.
- 81 J. G. Speight, in Handbook of Industrial Hydrocarbon Processes, Gulf Professional Publishing, 2011, pp. 1-41.
- 82 L. C. Chow, Monogr. Oral Sci., 2001, 18, 94-111.
- 83 E. Boanini, F. Silingardi, M. Gazzano and A. Bigi, Cryst. Growth Des., 2021, 21, 1689-1697.
- 84 P. N. Gavryushkin, N. Sagatov, A. B. Belonoshko, M. V. Banaev and K. D. Litasov, J. Phys. Chem. C, 2020, 124, 26467-26473.
- 85 L. H. Fu, Y. Y. Dong, M. G. Ma, W. Yue, S. L. Sun and R. C. Sun, Ultrason. Sonochem., 2013, 20, 1188-1193.
- 86 L. Pérez-Villarejo, F. Takabait, L. Mahtout, B. Carrasco-Hurtado, D. Eliche-Quesada and P. J. Sánchez-Soto, Ceram. Int., 2018, 44, 5291-5296.
- 87 J. Li and X. Li, *Energies*, 2019, **12**, 1–16.